Received: 11 July 2018 | Revised: 19 November 2018 | Accepted: 20 November 2018

DOI: 10.1002/mrm.27636

NOTE

Magnetic Resonance in Medicine

Non-contrast myocardial infarct scar assessment using a hybrid native T_1 and magnetization transfer imaging sequence at 1.5T

Chong Duan[1] | **Yanjie Zhu**[1,2] | **Jihye Jang**[1,3] | **Jennifer Rodriguez**[1] | **Ulf Neisius**[1] | **Ahmed S. Fahmy**[1] | **Reza Nezafat**[1]

[1]Department of Medicine (Cardiovascular Division), Beth Israel Deaconess Medical Center and Harvard Medical School, Boston, Massachusetts

[2]Paul C. Lauterbur Research Center for Biomedical Imaging, Shenzhen Institutes of Advanced Technology, Chinese Academy of Sciences, Shenzhen, China

[3]Department of Computer Science, Technical University of Munich, Munich, Germany

Correspondence
Reza Nezafat, Beth Israel Deaconess Medical Center, 330 Brookline Ave., Boston, MA 02215.
Email: rnezafat@bidmc.harvard.edu

Funding information
National Institutes of Health, Grant/Award Numbers: R01HL129185 and R01HL129157; American Heart Association, Grant/Award Number: 15EIA22710040.

Purpose: To develop a gadolinium-free cardiac MR technique that simultaneously exploits native T_1 and magnetization transfer (MT) contrast for the imaging of myocardial infarction.

Methods: A novel hybrid T one and magnetization transfer (HYTOM) method was developed based on the modified look-locker inversion recovery (MOLLI) sequence, with a train of MT-prep pulses placed before the balanced SSFP (bSSFP) readout pulses. Numerical simulations, based on Bloch-McConnell equations, were performed to investigate the effects of MT induced by (1) the bSSFP readout pulses, and (2) the MT-prep pulses, on the measured, "apparent," native T_1 values. The HYTOM method was then tested on 8 healthy adult subjects, 6 patients, and a swine with prior myocardial infarction (MI). The resulting imaging contrast between normal myocardium and infarcted tissues was compared with that of MOLLI. Late gadolinium enhancement (LGE) images were also obtained for infarct assessment in patients and swine.

Results: Numerical simulation and in vivo studies in healthy volunteers demonstrated that MT effects, resulting from on-resonance bSSFP excitation pulses and off-resonance MT-prep pulses, reduce the measured T_1 in both MOLLI and HTYOM. In vivo studies in patients and swine showed that the HYTOM sequence can identify locations of MI, as seen on LGE. Furthermore, the HYTOM method yields higher myocardium-to-scar contrast than MOLLI (contrast-to-noise ratio: 7.33 ± 1.67 vs. 3.77 ± 0.66, $P < 0.01$).

Conclusion: The proposed HYTOM method simultaneously exploits native T_1 and MT contrast and significantly boosts the imaging contrast for myocardial infarction.

KEYWORDS
Bloch-McConnell equations, magnetization transfer, MOLLI, myocardial infarction, native T_1

1 | INTRODUCTION

Myocardial infarction (MI) is the leading cause of morbidity in the United States with more than 1.2 million people experiencing MI per year.[1] In patients with prior MI, the risk of sudden cardiac death or major adverse complications, such as heart failure, have been directly related to various MI characteristics including infarct size, location, and transmurality.[2-5] Cardiac MR (CMR) offers high reproducibility and accuracy, allowing both functional assessment and characterization of myocardial tissue.[6] Late gadolinium enhancement (LGE) CMR is the current clinical standard for evaluating MI in patients.[7,8] Nevertheless, the use of gadolinium (Gd)-based contrast agent is contraindicated in patients with severe renal impairment.[9,10] Further, recent data show dose-dependent Gd accumulations in the dentate nucleus and globus pallidus in the brain, even in patients with normal renal function.[11,12] Therefore, a CMR approach that could detect and characterize MI without exogenous Gd-based contrast agent is still warranted.

Native T_1 mapping, which by definition does not require Gd, has demonstrated the potential for assessing myocardial infarction. Messroghli et al.[13] first evaluated the feasibility of using pre-contrast myocardial T_1 maps for characterizing MI at 1.5T and showed that native T_1 maps enable the detection of acute MI. Nevertheless, the limited native T_1 contrast between normal myocardium and chronic MI at 1.5T leads to poor diagnostic accuracy for chronic MI. Recently, there is emerging data that native T_1 mapping at 3T provides significantly greater sensitivity and specificity for chronic MI over native T_1 mapping at 1.5T and can reliably determine the location, size, and transmurality of chronic MI.[14,15] The performance of native T_1 mapping on characterizing MI has also been validated in animal models.[16-18] The heightened native T_1 values of MI observed in those studies have been ascribed to increased extracellular volume (ECV) fractions resulting from the edematous and fibrotic myocardium[19] and enhanced water proton diffusion.[20,21]

Besides native T_1, water–macromolecular proton magnetization transfer (MT) has long been used to enhance contrast between normal and infarcted tissue[22,23] and between blood and healthy myocardium[24-26] using off-resonance MT preparation pulses. Weber et al.[27] assessed MT effects in MI based on 2 sets of balanced SSFP (bSSFP) images with different levels of RF power deposition, which are achieved by varying the RF excitation pulse length while keeping the flip angle constant. In contrast, dual-flip angle bSSFP images have also been used to exploit MT effects in MI,[28,29] and the normalized signal differences between those bSSFP images were found to be strongly correlated with standard LGE measures.[28]

Interestingly, longitudinal relaxation and magnetization transfer are well known to be closely associated.[30,31] In fact, Robson et al.[32] demonstrated that MT effects resulting from bSSFP readout pulses reduce the myocardium T_1 when measured with the modified look-lock inversion recovery (MOLLI)[33] technique and showed that this bias can ironically improve the sensitivity of MOLLI to MI. This is because MI tissues, with reduced MT effect,[27,28] contribute less to the measured T_1 than the normal myocardium, therefore enhancing the contrast between normal and infarcted tissues. Nevertheless, this contrast improvement is small (~3% as estimated in Robson et al.[32]) because of the limited MT weighting introduced by the short on-resonance bSSFP excitation pulses.

In the present study, we aim to improve the native T_1 contrast between MI and remote myocardium at 1.5T. We hypothesize that the MT effects in MI tissues could be further exploited via additional long off-resonance MT-preparation pulses. We present a new sequence named hybrid T one and magnetization transfer (HYTOM). In HYTOM, an apparent longitudinal relaxation time constant, containing hybrid native T_1 and MT contrasts, is estimated voxel-wisely as a new imaging biomarker for the detection of MI. Numerical simulation, phantom studies, and in vivo studies in an animal model and patients with prior MI were carried out to investigate the performance of the proposed method.

2 | METHODS

2.1 | HYTOM sequence

To simultaneously exploit native T_1 and magnetization transfer contrast for MI imaging, a novel HYTOM sequence was proposed based on the 5-(3s)-3 MOLLI sequence for myocardium T_1 mapping.[34] In the proposed sequence, a train (N = 1–8) of off-resonance MT-preparation pulses were applied before the bSSFP readout modules within the MOLLI sequence (Figure 1). Sinc-Gaussian-shaped MT-preparation RF pulses were used with the following parameters: $\tau = 20$ ms, flip angle = 800º, off-resonance frequency = 500 Hz, and B_1 amplitude = 15.2 μT. A spoiler gradient was applied along the z direction following the MT-prep pulses to crush all residual transverse magnetization before the bSSFP readout.

2.2 | Numerical simulation with MT exchange

The Bloch-McConnell (BM) equations[35,36] are a general form for describing systems that are coupled via an exchange process. In the present study, cardiac tissue was modeled using the classic spin-bath model governed by the BM equations.[30] The spin-bath model consists of 2 pools of protons labeled as free pool (subscript f) and restricted pool (subscript r), with thermal equilibrium magnetization $M_{0,f} = (1-f)M_0$ and $M_{0,r} = fM_0$, respectively. M_0 is the total magnetization, and f

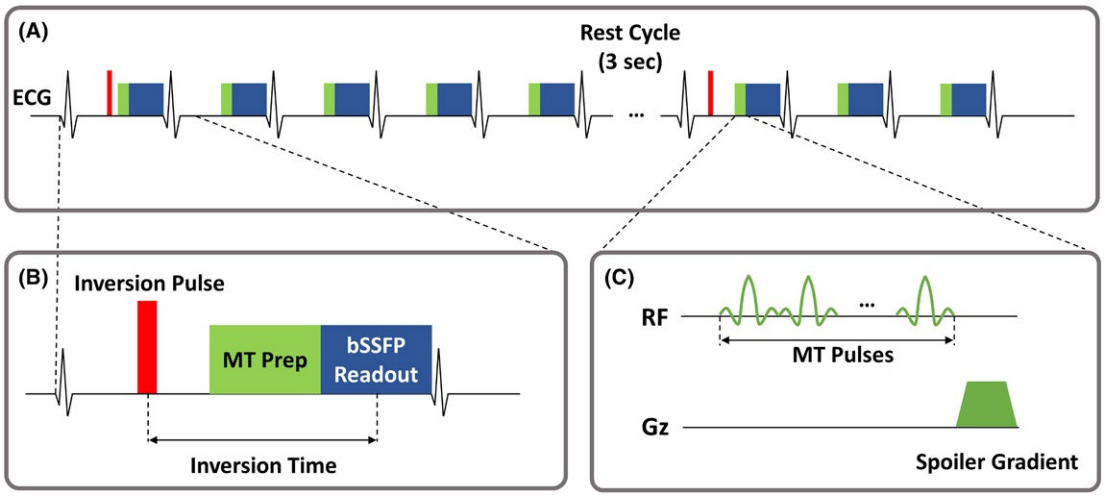

FIGURE 1 A, The proposed HYTOM pulse sequence consists of 2 sets of look-locker (LL) experiments separated by a 3-s rest cycle. B, An inversion pulse (only for the first acquisition of each LL), MT-prep module, and bSSFP readout module are placed within each heart beat cycle. Images are acquired at end-diastole via a specific ECG trigger delay. C, The MT-prep module consists of a train of Sinc-Gaussian off-resonance pulses, followed by a spoiler gradient along z at the end

is the fraction in the restricted pool (also known as semi-solid pool).

The MT effect is commonly described with a modification to the standard BM equations assuming the semi-solid pool has no transverse magnetization component because of the extremely short $T_{2,r}$ (on the order of 10 μs),[37] leading to 4 coupled differential equations for the system:

$$\frac{dM_{x,f}}{dt} = -R_{2,f}M_{x,f}, \tag{1}$$

$$\frac{dM_{y,f}}{dt} = -R_{2,f}M_{y,f} + \omega_1(t)M_{z,f}, \tag{2}$$

$$\frac{dM_{z,f}}{dt} = R_{1,f}\left(M_{0,f} - M_{z,f}\right) - k_f M_{z,f} + k_r M_{z,r} - \omega_1(t)M_{y,f}, \tag{3}$$

$$\frac{dM_{z,r}}{dt} = R_{2,r}\left(M_{0,b} - M_{z,b}\right) + k_f M_{z,f} - k_r M_{z,r} - W(\Delta,t)M_{z,r}. \tag{4}$$

In these equations, k_f and k_r are the exchange rate between the 2 pools. They are related *via* $k_f M_{0,f} = k_r M_{0,r}$ to preserve mass balance at thermal equilibrium. $\omega_1(t)$ is the excitation field strength ($\omega_1(t) = \gamma B_1(t)$). $W(\Delta, t)$ denotes an additional rate at which the z-component of the restricted pool is saturated by the applied RF pulses, and it is a function of the frequency (Δ) and amplitude ($B_1(t)$) of the RF pulses:

$$W(\Delta, t) = \frac{\pi\gamma^2}{\tau}\int_0^\tau B_1^2(t)dtG(\Delta), \tag{5}$$

where G describes the line shape for the restricted pool. A Super-Lorentzian line shape function was used here for the restricted pool consistent with the literature.[38]

In the present study, the extended phase graph framework[39,40] was used to simulate the effects of MT on: (1) the bSSFP transient and steady state signal, (2) the off-resonance profile of bSSFP, and (3) the longitudinal relaxation curve of look-locker-like sequences (i.e., MOLLI and HYTOM). MT effects arising from on-resonance bSSFP excitation pulses and off-resonance MT-prep pulses were both considered. Details of the simulation parameter values are given in Supporting Information Table S1.

2.3 | In vivo study

To develop and evaluate the performance of HYTOM, we imaged 8 healthy adult subjects (30 ± 14 y, 8 females), 6 patients (66 ± 10 y, 1 female), and 1 swine. We prospectively recruited 6 patients with prior MI to participate in our study. Each patient had 1 MI, and the duration between MI and CMR examination was 15.7 ± 6.3 (min: 10.2; max: 24.5) months. More details on these patients are given in Supporting Information Table S2. One Yorkshire swine underwent 180-min occlusion of the left anterior descending coronary artery to create an infarct.[18,41] This swine was then allowed to recover for 4 weeks before imaging. All in vivo experiments were performed on a Philips Achieva 1.5T scanner (Best, The Netherlands) with a 32-channel cardiac receiver coil array. All protocols were approved by Institutional Review Board and are HIPPA-compliant. The animal study was approved by the Institutional Animal Care and Use Committee. All human subjects provided written, informed consent to

participate in this study approved by the Institution's Human Subjects Committee.

For each subject, the imaging protocol included: (1) 5-(3s)-3 MOLLI sequence with the following typical parameters: TR/TE = 2.7/1.37 ms, FOV = 320 × 320 mm^2, acquisition matrix = 152 × 152, voxel size = 2.1 × 2.1 mm^2, linear phase-encoding ordering, SENSE factor = 2, slices = 3, slice thickness = 8 mm, bandwidth = 1880 Hz/pixel, and flip angle = 35°; and (2) HYTOM sequence with the following parameters for the off-resonant MT-preparation pulses: $\tau = 20$ ms, flip angle = 800°, off-resonance frequency = 500 Hz, B_1 amplitude = 15.2 μT, number of pulses N = 1, 2, 4, 6, and 8 (for healthy volunteers, i.e., 5 HYTOM scans for each subject) or N = 4 (for patients and swine). Four MT-prep pulses were used on patients and swine to optimize SNR and myocardium-to-scar contrast (see Discussion). Other imaging parameters were similar to those of the MOLLI sequence; (3) 3D LGE sequence (for patients and swine only) with the following typical parameters: TR/TE = 5.6/2.7 ms, flip angle = 15°, FOV = 360 – 400 × 360 – 400 × 120 mm^3, sensitivity encoding rate = 2.3, acquisition voxel size = 1.5 × 1.5 × 10 mm^3, slices = 20, acquisition window = 115 ms, low-high phase-encoding order, with 10 startup RF pulses to establish steady-state magnetization, 17 phase encoding lines per cardiac cycle, and spectral pre-saturation inversion recovery-based fat suppression. All in vivo images were acquired during the diastolic rest period. MOLLI and HYTOM were performed with breath-hold before contrast agent administration. Free-breathing LGE images were acquired 15–20 min after the intravenous administration of a bolus of 0.15 mmol/kg Gadobutrol (Bayer Healthcare, Berlin, Germany). A 2D pencil beam navigator with adaptive gating window size[42] was used to reduce respiratory motion artifacts in LGE images.

2.4 | Data analysis

The in vivo data sets were quantitatively analyzed to investigate the effect of MT-prep pulses on the measured apparent longitudinal relaxation rate and to compare the imaging contrast, between normal and infarcted myocardium, from the MOLLI and HYTOM sequences. All images were transferred to a separate workstation (ThinkStation P500, Lenovo Group Ltd., Hong Kong) for analysis. T_1 (and MT)-weighted images were first registered retrospectively using a nonrigid image registration algorithm[43] to compensate for residual in-plane motion. On registration, voxel-wise curve fitting was performed to generate T_1 maps using a 3-parameter fitting model followed by look-locker correction as described in Messroghli et al.[33] For healthy volunteers, regions of interest (ROIs) were manually drawn on the septum. For each patient and swine, ROIs of the infarct were defined by an experienced cardiologist (U.N. with 11 years of experience in cardiovascular imaging) on MOLLI, HYTOM, and LGE images. Following Kali et al.[15] contrast-to-noise ratios (CNRs) were calculated for the 3 techniques as follows:

$$CNR_{LGE} = \frac{SI_{\text{infarct}} - SI_{\text{normal}}}{\sigma_{\text{noise}}}, \tag{6}$$

$$CNR_{MOLLI} = \frac{T_{1,\text{infarct}} - T_{1,\text{normal}}}{\sigma_{T_{1,\text{normal}}}}, \tag{7}$$

$$CNR_{HYTOM} = \frac{\text{Apparent}T_{1,\text{infarct}} - \text{Apparent}T_{1,\text{normal}}}{\sigma_{\text{Apparent}T_{1,\text{normal}}}}. \tag{8}$$

All simulation and data analysis were performed using MATLAB (version 2017b; The MathWorks, Natick, MA). The simulation source code is available at https://github.com/chongduan/HYTOM. Codes for all simulation results presented in this article are included (hash 78b54d7 was the version at time of submission). Infarct size and transmurality were quantified using the freely available software Segment v2.2 (http://segment.heiberg.se). The measured apparent T_1 values and the CNRs as defined by Equations 6–8 from MOLLI, HYTOM, and LGE were compared using a paired-sample Student's t-test. Statistical significance was defined at $P < 0.05$.

3 | RESULTS

Figure 2 shows numerical simulation results for magnetization transfer effects. Figure 2A illustrates the approach to steady-state of bSSFP readout sequence in 3 scenarios: (1) single-pool model (free water only); (2) 2-pool model; and (3) the 2-pool model with additional off-resonant MT-preparation pulses placed ahead of the bSSFP readout (Figure 1). The MT effect, resulting from on-resonance bSSFP pulses, reduces both transient and steady state signals. The MT-prep pulses further enhance the signal difference at the transient phase. The 2-pool model and 2-pool model with MT-prep both approach the same steady state (inset in Figure 2A), which is ~5% lower than the single-pool model. Figure 2B shows the bSSFP off-resonance profiles simulated for the 3 scenarios described above at the center of k-space. The high frequency fluctuation observed in the 3 curves reflects a transient behavior of bSSFP, and it vanishes as the bSSFP signal approaches steady state. Figure 2C illustrates the corresponding apparent longitudinal relaxation curves for the 3 scenarios. Consistent with previous literature,[32,44] the MT effect from the bSSFP readout pulses alone contributes to the

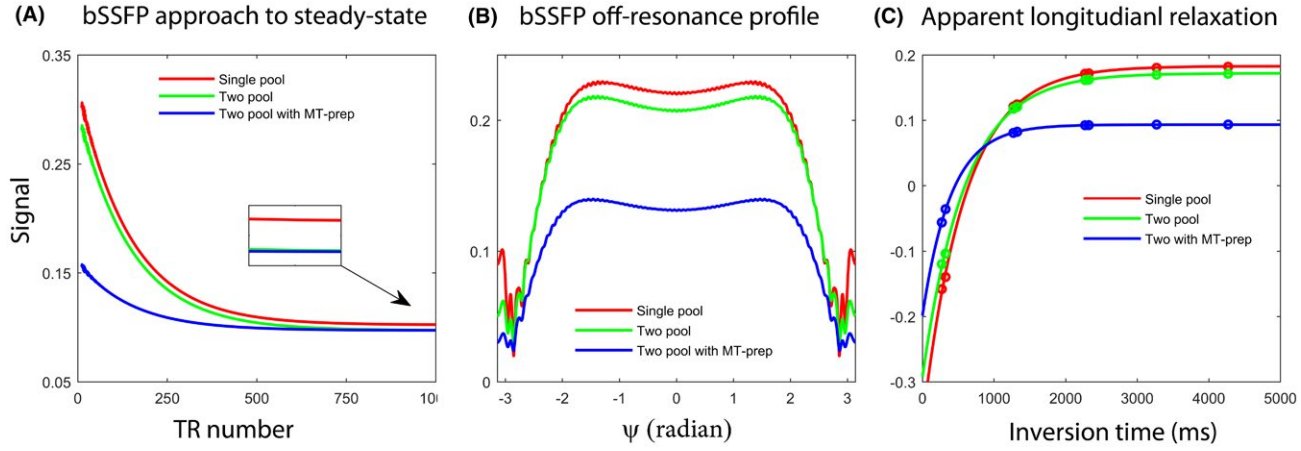

FIGURE 2 Numerical simulation illustrating the effect of magnetization transfer on the approach to bSSFP steady state A, bSSFP off-resonance signal profiles at the center of kspace (TR number = 40) B, and the apparent relaxation for LL-based sequences C. Red, green, and blue curves represent the cases of single pool (i.e., free water pool only), 2-pool (i.e., free water pool and restricted water pool), and 2 pool with MT-prep pulses, respectively. The inset in (A) shows a zoomed-in window at the steady state of the 3 scenarios

relaxation measured in MOLLI-like experiments, leading to a 13% decrease of T_1. This result is in excellent agreement with that shown by Robson et al.[32] obtained with a different simulation approach. In the present study, the additional MT-prep further enhanced the MT effects (blue curve), leading to a 27% change in the measured relaxation time constant.

Following simulation, we tested the hypothesis that MT-prep pulses can reduce the apparent relaxation time measured with HYTOM sequence in phantom (Supporting Information Figure S1) and healthy volunteers (Supporting Information Figures S2 and S3). Supporting Information Figure S1 shows that the MT-prep pulses ($N = 4$) induces an 18% decrease in the measured T_1 by HYTOM comparing to MOLLI for a 2.3% agarose solution, whereas the measured T_1 only changes ~0.6% for tap water (i.e., no MT effect). Supporting Information Figure S2 shows the T_1-weighted images and reconstructed apparent T_1 maps for a representative healthy volunteer based on the standard MOLLI and proposed HYTOM sequences. Note the different contrasts, because of additional MT-weighting, between the myocardium and blood pool on the raw T_1-weighted images for MOLLI and HYTOM. Consistent with the simulations and phantom results, HYTOM produces lower measured T_1 values than MOLLI, and this difference is a function of the number of MT pulses (i.e., off-resonance irradiation time) as shown in Supporting Information Figure S3 and Supporting Information Table S3.

Figure 3 shows a comparison between LGE, MOLLI, and HYTOM sequences in a swine model with infarct. Both MOLLI and HYTOM methods demonstrate heightened-apparent native T_1 values in close spatial agreement with the standard LGE images. More importantly, because of the additional magnetization transfer contrast in HYTOM, the measured T_1 values of normal myocardium with higher MT effect is further suppressed, leading to better contrast between the infarcted and normal myocardium relative to MOLLI. Accuracies of infarct size measured by MOLLI and HYTOM are 74 ± 16% and 78 ± 12%, respectively, assuming LGE is the ground truth.

Similar to the results of the animal study, Figure 4 demonstrates that HYTOM affords better identification of MI than the MOLLI sequence in 2 representative patients with prior MI. Further, infarct sizes measured by HYTOM and MOLLI correlates well with that measured by LGE (HYTOM vs. LGE: $R^2 = 0.986$, slope = 0.896, intercept = −0.002; MOLLI vs. LGE: $R^2 = 0.997$, slope = 0.658, intercept = 0.005). HYTOM has a higher accuracy than MOLLI (84 ± 8% vs. 76 ± 11%, $P < 0.01$). Similarly, transmurality measured by HYTOM and MOLLI also correlates well with that measured by LGE (HYTOM vs. LGE: $R^2 = 0.979$, slope = 0.740, intercept = 5.08; MOLLI vs. LGE: $R^2 = 0.974$, slope = 0.599, intercept = 9.09). Both HYTOM and MOLLI underestimate the infarct transmurality compared to LGE (LGE: 43.2 ± 17.8%; HYTOM: 37.06 ± 13.30%; MOLLI: 34.99 ± 10.8%).

Figure 5A illustrates the apparent T_1 values as measured by MOLLI and HYTOM for remote normal and infarcted myocardium. In MOLLI, the scarred tissues have higher apparent native T_1 values than the normal myocardium (1336 ± 37 ms vs. 1102 ± 40 ms, $P < 0.01$). In HYTOM, the additional MT-weighting has a greater reductive impact on the measured apparent T_1 value for the normal myocardium than for the infarcted myocardium (1289 ± 38 ms vs. 937 ± 28 ms, $P < 0.01$). The HYTOM method yields larger differences in apparent T_1 values between infarct scar and remote myocardium than MOLLI (352 ± 19 ms vs. 234 ± 37 ms, $P < 0.01$). Figure 5B shows that HYTOM has a better contrast-to-noise ratio (CNR) than

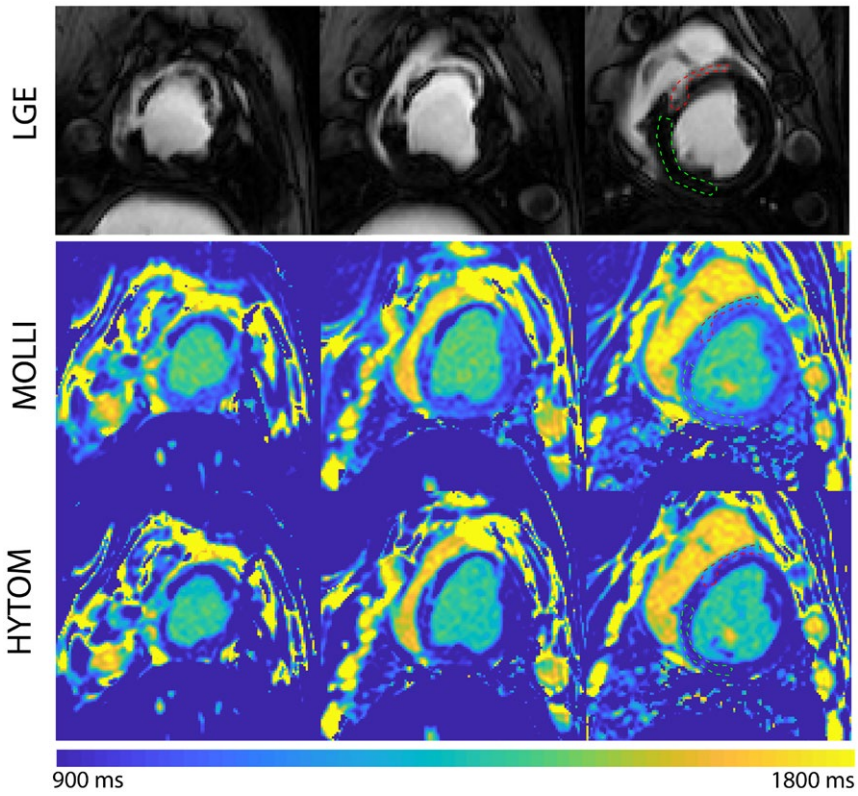

FIGURE 3 Comparison of LGE (top), MOLLI (middle), and HYTOM (bottom) for 3 slices (left to right columns) from a swine with infarct, demonstrating improvements in the MI contrast of HYTOM relative to MOLLI. Red and green dashed circles show representative ROIs for infarcted and normal myocardium, respectively

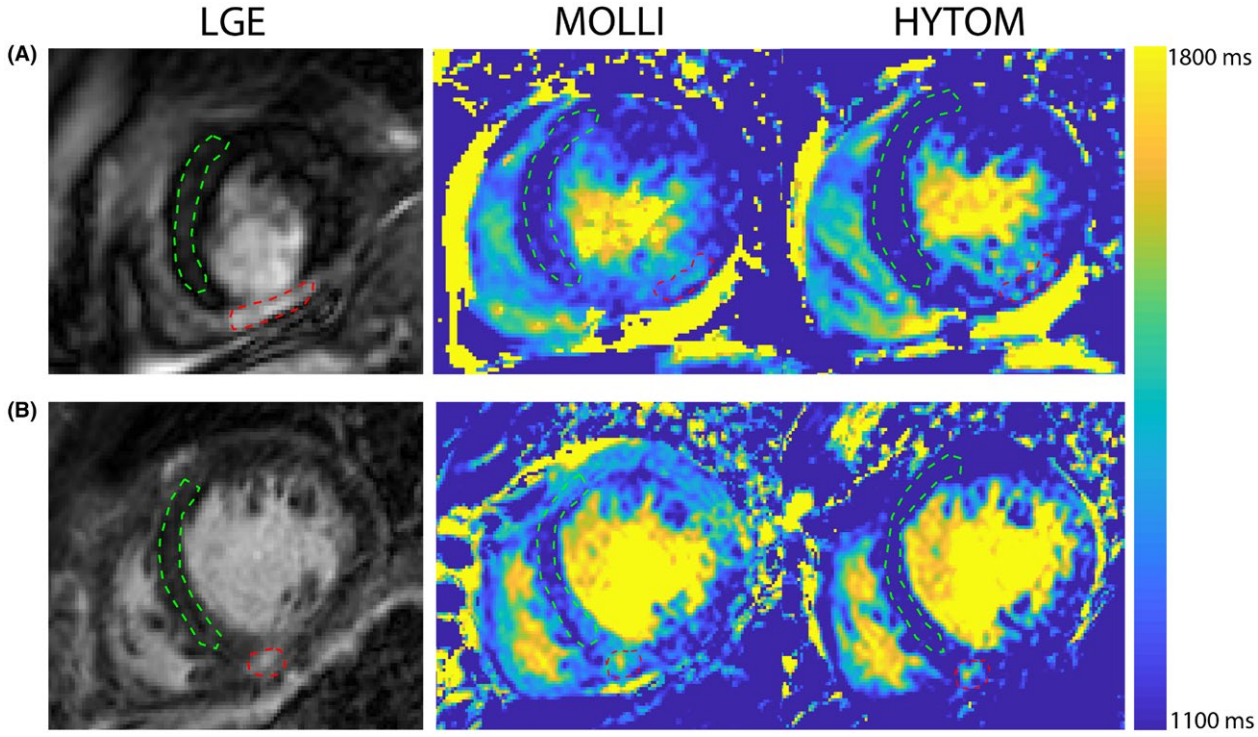

FIGURE 4 Comparison of LGE (left column), MOLLI (middle column), and HYTOM (right column) images in 2 patients (A and B) with prior MI. Similar to Figure 3, red and green dashed circles indicate the ROIs for infarcted and normal myocardium, respectively

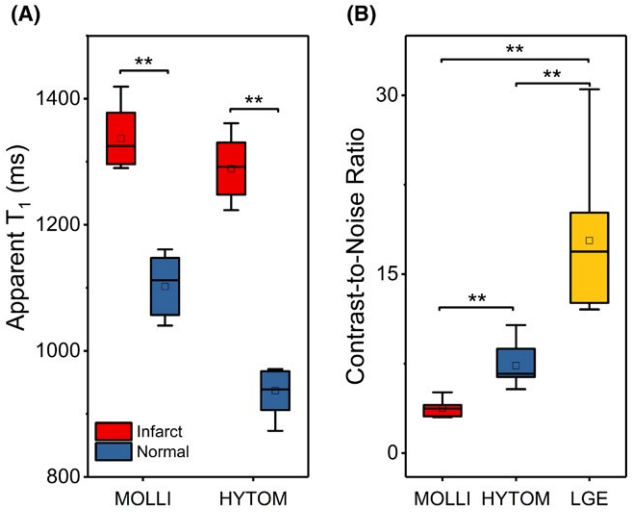

FIGURE 5 A, Apparent T_1 values of normal and infarcted tissues ($N = 7$) as estimated by MOLLI (left pair) and HYTOM (right pair). B, CNRs in MOLLI, HYTOM, and LGE as defined by Equations 6–8. $^{**}P < 0.01$ and $^{***}P < 0.001$ as measured by a paired-sample t-test

MOLLI (7.33 ± 1.67 vs. 3.77 ± 0.66, $P < 0.01$), whereas LGE has the highest CNR among the 3 methods (17.8 ± 5.84, $P < 0.001$).

4 | DISCUSSION

In this work, the HYTOM method for imaging myocardial infarction is presented. In HYTOM, an apparent longitudinal relaxation time constant is estimated after applying off-resonance MT-prep pulses in the context of myocardium T_1 mapping. This resulting apparent T_1 value simultaneously exploits native T_1 and MT contrasts, which significantly improves the contrast for MI without the need of an exogenous Gd-based contrast agent.

Myocardial T_1 mapping by MOLLI and its variants has proven to be a powerful method of evaluating diseased hearts in the absence of exogenous contrast media.[45,46] Nevertheless, there have been well-known inconsistencies in the measured T_1 values between those methods and the gold-standard measurements (e.g., conventional inversion recovery spin-echo methods).[44] Furthermore, MOLLI has been widely known to underestimate T_1 in in vivo studies relative to SASHA,[47] SAPPHIRE,[48] or STONE,[49,50] which are believed to be more accurate methods.[51] The biases in MOLLI-like methods are partially attributed to the magnetization transfer effect that can occur by direct chemical exchange or indirect dipole-medicated cross-relaxation in the myocardium.[52]

In the present study, we demonstrate that MT-induced biases can be harnessed to improve the contrast in MI imaging via application of long off-resonance MT-prep pulses. We have shown that the proposed HYTOM affords better CNR than MOLLI, even though its CNR is still lower than that of LGE (Figure 5). Because MOLLI and HYTOM have approximately the same total scan time, it follows that HYTOM also has higher CNR efficiency (i.e., CNR per unit time) than MOLLI. We note that the MOLLI T_1 difference between infarct and remote zones in the present study is larger than that reported by Messroghli et al.[13] This is likely because the infarct ROIs were defined differently. In Messroghli et al.[13] the ROIs were defined on delayed-enhancement images and then copied onto native T_1 maps, whereas in the present study a cardiologist defined ROIs directly on native T_1 maps. It is well-known that LGE has a higher sensitivity for detecting infarcts than MOLLI at 1.5T and therefore estimates larger infarct–lesion volumes. As a result, the average native T_1 values across a larger volume defined on LGE images is smaller, and therefore the T_1 difference is smaller. As mentioned earlier, in addition to off-resonance preparation pulses, MT effects can also be exploited by modulating the on-resonance bSSFP excitation pulses.[27,28] It follows that MI contrast could, in theory, be further improved by optimizing both off-resonance preparation pulses and on-resonance readout pulses. On the other hand, several studies have demonstrated that native T_1 mapping at 3T provides significantly greater sensitivity for MI over native T_1 mapping at 1.5T[14,15] because of the T_1 elongations at 3T.[53] Similarly, the proposed HYTOM method, with a hybrid native T_1 and MT contrast, also benefits from higher fields. The MT effect also increases with increasing field strength,[54] which could further contribute to myocardium-to-scar contrast in HYTOM. Future work is needed to identify the optimal pulse sequence parameters for the proposed HYTOM method and investigate its performance at a higher field.

It is worth noting that MT-induced bias in native T_1 mapping positively correlates to off-resonance MT-prep time (Supporting Information Figure S3). In this respect, a longer MT-prep time should result in better myocardium-to-scar contrast. In practice, direct saturation of the free water pool by MT preparation pulses is inevitable, and significantly reduces the SNR at longer preparation time. This explains the increased variance in the estimated apparent T_1 (Supporting Information Figure S3). Besides SNR, the additional specific absorption rate (SAR) caused by MT pulses also limits the extent of contrast that can be achieved via HYTOM, particularly at high field strengths.

Myocardial infarction and subsequent infarct healing are complex and heterogeneous processes, which involve disruption of myofibrils, inflammatory cell infiltration, interstitial edema, production of collagen by fibroblasts, and eventually scar formation.[55,56] Even though many studies have demonstrated the decreased MT effects in both acute and chronic MI

tissues,[22,23,27,28,37] the specific tissue changes that resulted in the observed decrease remain to be determined. It is interesting that even though the loss of myocytes and increased ECV in infarcted tissues are consistent with the decrease in MT, the extensive collagen depositions seems counter intuitive. However, it is worthwhile to note that, besides macromolecular contents in the myocardium, the MT effects directly depend on the coupling between H_f (i.e., free water pool protons) and H_r (i.e., restricted water pool protons), which reflects changes in the macromolecular surface chemistry or surface dynamics.[57] As pointed out by Scholz et al.[22] the observed decrease in MT in chronic MI tissues may suggest that membrane, structural, and contractile proteins of the normal myocardium provide more suitable surface chemistry for magnetization transfer (i.e., the H_f–H_r coupling). Further work is still needed to tease out the detailed molecular mechanisms of magnetization transfer occurring in infarcted tissues.

There are several limitations in the current study. First, the proposed HYTOM method was evaluated on a small sample size of subjects with different spatial coverages and resolutions compared to LGE. Second, there are some differences in the hyper-intensity regions between LGE and HYTOM (this limitation also exists with MOLLI). These inconsistencies are likely because of motion artifacts (e.g., lateral wall hyper-intensity region in Figure 4B), inflammation and/or edema (Figure 3 and Supporting Information Figure S4), and the inherent differences in contrast mechanisms. Nevertheless, it will be interesting to evaluate magnetization transfer contrast in HYTOM by quantifying the restricted pool fraction and exchange rate constant, which might provide new insights into the complex post-infarction remodeling processes.

5 | CONCLUSION

To conclude, the proposed HYTOM method simultaneously exploits native T_1 and magnetization transfer in infarcted myocardial tissues and therefore offers an improved contrast for detection and characterization of MI without Gd-based contrast agents. Further efforts will be focused on evaluating and optimizing HYTOM for longitudinal characterization of MI in animal models and patients.

ACKNOWLEDGMENTS

We thank Sophie Berg, RN, Beth Goddu, RT, and Patrick Pierce, RT, for their help with patient recruitment and scanning of animals and patients. We acknowledge the grant support from the National Institutes of Health (R01HL129185 and R01HL129157), and the American Heart Association (15EIA22710040). Yanjie Zhu is funded by the National Natural Science Foundation of China (61771463 and 81830056).

ORCID

Chong Duan https://orcid.org/0000-0001-9817-5340
Yanjie Zhu https://orcid.org/0000-0002-9131-689X

REFERENCES

1. Mozaffarian D, Benjamin EJ, Go AS, et al. Heart disease and stroke statistics—2016 update: a report from the American Heart Association. *Circulation*. 2016;133:e38–e360.
2. Bello D, Fieno DS, Kim RJ, et al. Infarct morphology identifies patients with substrate for sustained ventricular tachycardia. *J Am Coll Cardiol*. 2005;45:1104–1108.
3. Ashikaga H, Sasano T, Dong J, et al. Magnetic resonance–based anatomical analysis of scar-related ventricular tachycardia: implications for catheter ablation. *Circ Res*. 2007;101:939–947.
4. Rayatzadeh H, Tan A, Chan RH, et al. Scar heterogeneity on cardiovascular magnetic resonance as a predictor of appropriate implantable cardioverter defibrillator therapy. *J Cardiovasc Magn Reson*. 2013;15:31.
5. Lee DC, Goldberger JJ. CMR for sudden cardiac death risk stratification: are we there yet? *JACC Cardiovasc Imaging*. 2013;6:345–348.
6. Pennell DJ. Cardiovascular magnetic resonance. *Circulation*. 2010;121:692–705.
7. Kim RJ, Fieno DS, Parrish TB, et al. Relationship of MRI delayed contrast enhancement to irreversible injury, infarct age, and contractile function. *Circulation*. 1999;100:1992–2002.
8. Kim RJ, Wu E, Rafael A, et al. The use of contrast-enhanced magnetic resonance imaging to identify reversible myocardial dysfunction. *N Engl J Med*. 2000;343:1445–1453.
9. Kuo PH, Kanal E, Abu-Alfa AK, Cowper SE. Gadolinium-based MR contrast agents and nephrogenic systemic fibrosis. *Radiology*. 2007;242:647–649.
10. Sadowski EA, Bennett LK, Chan MR, et al. Nephrogenic systemic fibrosis: risk factors and incidence estimation. *Radiology*. 2007;243:148–157.
11. Kanda T, Ishii K, Kawaguchi H, Kitajima K, Takenaka D. High signal intensity in the dentate nucleus and globus pallidus on unenhanced T1-weighted MR images: relationship with increasing cumulative dose of a gadolinium-based contrast material. *Radiology*. 2014;270:834–841.
12. Ramalho J, Castillo M, AlObaidy M, et al. High signal intensity in globus pallidus and dentate nucleus on unenhanced T1-weighted MR images: evaluation of two linear gadolinium-based contrast agents. *Radiology*. 2015;276:836–844.
13. Messroghli DR, Walters K, Plein S, et al. Myocardial T1 mapping: application to patients with acute and chronic myocardial infarction. *Magn Reson Med*. 2007;58:34–40.
14. Kali A, Cokic I, Tang RL, et al. Determination of location, size, and transmurality of chronic myocardial infarction without exogenous contrast media by using cardiac magnetic resonance imaging at 3 T. *Circ Cardiovasc Imaging*. 2014;7:471–481.
15. Kali A, Choi EY, Sharif B, et al. Native T1 mapping by 3-T CMR imaging for characterization of chronic myocardial infarctions. *JACC Cardiovasc Imaging*. 2015;8:1019–1030.
16. Liu X, Hou J, Zg Yang, et al. Native T1 mapping for characterization of acute and chronic myocardial infarction in swine:

comparison with contrast-enhanced MRI. *J Magn Reson Imaging*. 2018;47:1406–1414.
17. Cui C, Wang S, Lu M, et al. Detection of recent myocardial infarction using native T1 mapping in a swine model: a validation study. *Sci Rep*. 2018;8:7391.
18. Whitaker J, Tschabrunn CM, Jang J, et al. Cardiac MR characterization of left ventricular remodeling in a swine model of infarct followed by reperfusion. *J Magn Reson Imaging*. 2018. https://doi.org/10.1002/jmri.26005.
19. Bauner KU, Biffar A, Theisen D, et al. Extracellular volume fractions in chronic myocardial infarction. *Invest Radiol*. 2012;47:538–545.
20. Pop M, Ghugre NR, Ramanan V, et al. Quantification of fibrosis in infarcted swine hearts by ex vivo late gadolinium-enhancement and diffusion-weighted MRI methods. *Phys Med Biol*. 2013;58:5009.
21. Simpson J, Carr H. Diffusion and nuclear spin relaxation in water. *Phys Rev*. 1958;111:1201.
22. Scholz TD, Hoyt RF, Deleonardis JR, Ceckler TL, Balaban RS. Water-macromolecular proton magnetization transfer in infarcted myocardium: a method to enhance magnetic resonance image contrast. *Magn Reson Med*. 1995;33:178–184.
23. Weiss CR, Aletras AH, London JF, et al. Stunned, infarcted, and normal myocardium in dogs: simultaneous differentiation by using gadolinium-enhanced cine MR imaging with magnetization transfer contrast. *Radiology*. 2003;226:723–730.
24. Manning WJ, Nezafat R, Appelbaum E, Danias PG, Hauser TH, Yeon SB. Coronary magnetic resonance imaging. *Cardiol Clin*. 2007;25:141–170.
25. Nezafat R, Han Y, Peters DC, et al. Coronary magnetic resonance vein imaging: imaging contrast, sequence, and timing. *Magn Reson Med*. 2007;58:1196–1206.
26. Stoeck CT, Hu P, Peters DC, et al. Optimization of on-resonant magnetization transfer contrast in coronary vein MRI. *Magn Reson Med*. 2010;64:1849–1854.
27. Weber OM, Speier P, Scheffler K, Bieri O. Assessment of magnetization transfer effects in myocardial tissue using balanced steady-state free precession (bSSFP) cine MRI. *Magn Reson Med*. 2009;62:699–705.
28. Stromp TA, Leung SW, Andres KN, et al. Gadolinium free cardiovascular magnetic resonance with 2-point Cine balanced steady state free precession. *J Cardiovasc Magn Reson*. 2015;17:90.
29. Germain P, El Ghannudi S, Labani A, et al. A dual flip angle 3D bSSFP magnetization transfer-like method to differentiate between recent and old myocardial infarction. *J Magn Reson Imaging*. 2018;47:798–808.
30. Henkelman RM, Huang X, Xiang QS, Stanisz GJ, Swanson SD, Bronskill MJ. Quantitative interpretation of magnetization transfer. *Magn Reson Med*. 1993;29:759–766.
31. Prantner AM, Bretthorst GL, Neil JJ, Garbow JR, Ackerman JJ. Magnetization transfer induced biexponential longitudinal relaxation. *Magn Reson Med*. 2008;60:555–563.
32. Robson MD, Piechnik SK, Tunnicliffe EM, Neubauer S. T1 measurements in the human myocardium: the effects of magnetization transfer on the SASHA and MOLLI sequences. *Magn Reson Med*. 2013;70:664–670.
33. Messroghli DR, Radjenovic A, Kozerke S, Higgins DM, Sivananthan MU, Ridgway JP. Modified Look-Locker inversion recovery (MOLLI) for high-resolution T1 mapping of the heart. *Magn Reson Med*. 2004;52:141–146.
34. Kellman P, Arai AE, Xue H. T1 and extracellular volume mapping in the heart: estimation of error maps and the influence of noise on precision. *J Cardiovasc Magn Reson*. 2013;15:56.
35. Bloch F. Nuclear induction. *Phys Rev*. 1946;70:460.
36. McConnell HM. Reaction rates by nuclear magnetic resonance. *J Chem Phys*. 1958;28:430–431.
37. Graham SJ, Stanisz GJ, Kecojevic A, Bronskill MJ, Henkelman RM. Analysis of changes in MR properties of tissues after heat treatment. *Magn Reson Med*. 1999;42:1061–1071.
38. Morrison C, Henkelman RM. A model for magnetization transfer in tissues. *Magn Reson Med*. 1995;33:475–482.
39. Weigel M. Extended phase graphs: dephasing, RF pulses, and echoes - pure and simple. *J Magn Reson Imaging*. 2015;41:266–295.
40. Malik SJ, Teixeira R, Hajnal JV. Extended phase graph formalism for systems with magnetization transfer and exchange. *Magn Reson Med*. 2018;80:767–779.
41. Tschabrunn CM, Roujol S, Nezafat R, et al. A swine model of infarct-related reentrant ventricular tachycardia: electroanatomic, magnetic resonance, and histopathological characterization. *Heart Rhythm*. 2016;13:262–273.
42. Moghari MH, Chan RH, Hong SN, et al. Free-breathing cardiac MR with a fixed navigator efficiency using adaptive gating window size. *Magn Reson Med*. 2012;68:1866–1875.
43. Roujol S, Foppa M, Weingartner S, Manning WJ, Nezafat R. Adaptive registration of varying contrast-weighted images for improved tissue characterization (ARCTIC): application to T1 mapping. *Magn Reson Med*. 2015;73:1469–1482.
44. Kellman P, Hansen MS. T1-mapping in the heart: accuracy and precision. *J Cardiovasc Magn Reson*. 2014;16:2.
45. Kammerlander AA, Marzluf BA, Zotter-Tufaro C, et al. T1 mapping by CMR imaging: from histological validation to clinical implication. *JACC Cardiovasc Imaging*. 2016;9:14–23.
46. Ferreira VM, Wijesurendra RS, Liu A, et al. Systolic ShMOLLI myocardial T1-mapping for improved robustness to partial-volume effects and applications in tachyarrhythmias. *J Cardiovasc Magn Reson*. 2015;17:77.
47. Chow K, Flewitt JA, Green JD, Pagano JJ, Friedrich MG, Thompson RB. Saturation recovery single-shot acquisition (SASHA) for myocardial T(1) mapping. *Magn Reson Med*. 2014;71:2082–2095.
48. Weingärtner S, Akçakaya M, Basha T, et al. Combined saturation/inversion recovery sequences for improved evaluation of scar and diffuse fibrosis in patients with arrhythmia or heart rate variability. *Magn Reson Med*. 2014;71:1024–1034.
49. Weingärtner S, Roujol S, Akçakaya M, Basha TA, Nezafat R. Free-breathing multislice native myocardial T1 mapping using the slice-interleaved T1 (STONE) sequence. *Magn Reson Med*. 2015;74:115–124.
50. Jang J, Bellm S, Roujol S, et al. Comparison of spoiled gradient echo and steady-state free-precession imaging for native myocardial T1 mapping using the slice-interleaved T1 mapping (STONE) sequence. *NMR Biomed*. 2016;29:1486–1496.
51. Roujol S, Weingärtner S, Foppa M, et al. Accuracy, precision, and reproducibility of four T1 mapping sequences: a head-to-head comparison of MOLLI, ShMOLLI, SASHA, and SAPPHIRE. *Radiology*. 2014;272:683–689.
52. Hoffman RA, Forsén S. Transient and steady-state overhauser experiments in the investigation of relaxation processes. Analogies between chemical exchange and relaxation. *J Chem Phys*. 1966;45:2049–2060.

53. Stanisz GJ, Odrobina EE, Pun J, et al. T1, T2 relaxation and magnetization transfer in tissue at 3T. *Magn Reson Med*. 2005;54:507–512.
54. Henkelman RM, Stanisz GJ, Graham SJ. Magnetization transfer in MRI: a review. *NMR Biomed*. 2001;14:57–64.
55. Thygesen K, Alpert JS, Jaffe AS, et al. Third universal definition of myocardial infarction. *Eur Heart J*. 2012;33:2551–2567.
56. Frangogiannis NG. The inflammatory response in myocardial injury, repair, and remodelling. *Nat Rev Cardiol*. 2014;11:255–265.
57. Wolff SD, Balaban RS. Magnetization transfer contrast (MTC) and tissue water proton relaxation in vivo. *Magn Reson Med*. 1989;10:135–144.

SUPPORTING INFORMATION

Additional supporting information may be found online in the Supporting Information section at the end of the article.

FIGURE S1 Phantom study was performed to investigate the effect of off-resonance MT-prep pulses on the measured apparent T_1. A phantom with 9 vials of $NiCl_2$-doped agarose solutions (right), each with different agarose concentrations, and a tube of tap water (left) were imaged. Top row shows the measured T_1 maps for MOLLI (left) and HYTOM (right) sequences. Bottom row shows the relaxation curves of tap water (purple arrow) and 2.3% agarose (red arrow head) as measured by MOLLI and HYTOM methods. Note the enhanced longitudinal relaxation rate of the agarose solution (18%), whereas that of the tap water hardly changes (0.6%)

FIGURE S2 MOLLI and HYTOM images for a representative healthy volunteer demonstraing the effect of MT-prep pulses on the reconstrcuted T_1-weighted images and T_1 maps. Inversion times of T_1-weighted images in MOLLI are 150, 1138, 2134, 3896, 4792, 350, 1264, and 2219 ms; HYTOM: 1274, 2247, 3187, 4138, 350, 1289, and 2240 ms

FIGURE S3 The measured apparent T_1 as a function of the number of MT-prep pulses (i.e., off-resonance irradiation time) for a representative healthy volunteer (same as shown in Supporting Information Figure 2). The measured T_1 decreases as the number of MT pulses increases. Note that the variance of apparent T_1 also increases. This is because the MT-preparation pulses reduce the signal, and lower SNR images lead to higher variance in T_1 estimation

FIGURE S4 Comparison of LGE, MOLLI, HYTOM, and T_2 mapping for a patient (top row) and a swine (bottom row)

TABLE S1 Simulation parameter values

TABLE S2 Features of patients in in vivo study

TABLE S3 Regional analysis of MOLLI and HYTOM in healthy volunteers

How to cite this article: Duan C, Zhu Y, Jang J, et al. Non-contrast myocardial infarct scar assessment using a hybrid native T_1 and magnetization transfer imaging sequence at 1.5T. *Magn Reson Med*. 2018;00:1–10. https://doi.org/10.1002/mrm.27636